HHS Public Access

Author manuscript

J Chem Inf Model. Author manuscript; available in PMC 2023 March 27.

Published in final edited form as:

J Chem Inf Model. 2022 March 14; 62(5): 1249–1258. doi:10.1021/acs.jcim.1c01188.

Discovery of VapC1 small molecule nuclease inhibitors by virtual screening and scaffold hopping from an atomic structure revealing protein-protein interactions with native VapB1 inhibitor

Hongmao Sun[1], **Nathan P. Coussens**[1], **Carina Danchik**[1], **Leah M. Wachsmuth**[1], **Mark J. Henderson**[1], **Samarjit Patnaik**[1], **Matthew D. Hall**[1], **Ashley L. Molinaro**[2], **Dayle A. Daines**[2], **Min Shen**[1,*]

[1]National Center for Advancing Translational Sciences (NCATS), 9800 Medical Center Dr. Rockville, MD 20850

[2]Office of the Dean, College of Sciences, Old Dominion University, Norfolk, VA 23529, USA

Abstract

Nontypeable *Haemophilus influenzae* (NTHi) are clinically important Gram-negative bacteria that are responsible for various human mucosal diseases, including otitis media (OM). Recurrent OM caused by NTHi is common and infections which recur less than two weeks following antimicrobial therapy are largely attributable to recurrence of the same strain of bacteria. Toxin-antitoxin (TA) modules encoded by bacteria enable rapid responses to environmental stresses and are thought to facilitate growth arrest, persistence, and tolerance to antibiotics. The *vapBC-1* locus of NTHi encodes a type II TA system, comprising the ribonuclease toxin VapC1 and its cognate antitoxin VapB1. The activity of VapC1 has been linked to the survival of NTHi during antibiotic treatment both *in vivo* and *ex vivo*. Therefore, inhibitors of VapC1 might serve as adjuvants to antibiotics, preventing NTHi from entering growth arrest and surviving; however, none have been reported to date. A truncated VapB1 peptide from a crystal structure of the VapBC-1 complex was used to generate pharmacophore queries to facilitate a scaffold hopping approach for the identification of small molecule VapC1 inhibitors. The National Center for Advancing Translational Sciences small molecule library was virtually screened using the shape-based method Rapid Overlay of Chemical Structures (ROCS) and the top-ranking hits were docked into the VapB1 binding pocket of VapC1. Two hundred virtual screening hits with the best docking scores were selected and tested in a biochemical VapC1 activity assay, which confirmed eight compounds as VapC1 inhibitors. An additional sixty compounds were selected with structural similarities to the confirmed VapC1 inhibitors, of which twenty inhibited VapC1 activity. Intracellular target engagement of five inhibitors was indicated by the destabilization of VapC1 within bacterial cells from a cellular thermal shift assay; however, no impact on bacterial growth was observed. Thus, this virtual screening and scaffold hopping approach enabled the discovery of VapC1 ribonuclease inhibitors that might serve as starting points for preclinical development.

[*]Contact information for the corresponding author: Min Shen, PhD, shenmin@mail.nih.gov.

Supporting information: ID, structure and IC_{50} of the 28 virtual screening hits.

Conflicts of Interest: The authors declare no conflicts of interest.

Graphical Abstract

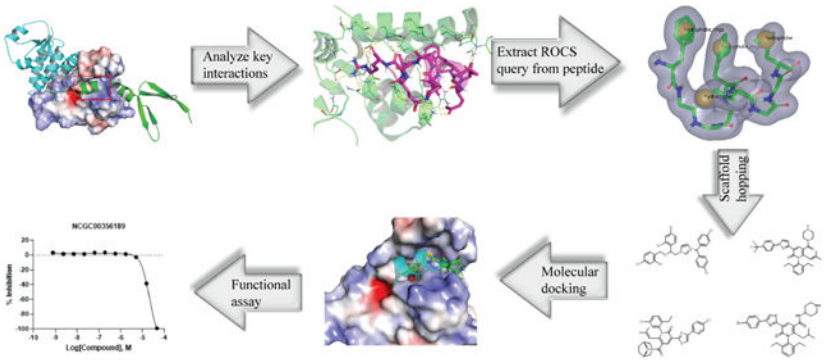

Introduction

The pleomorphic Gram-negative bacteria nontypeable *Haemophilus influenzae* (NTHi) are human-adapted commensals residing in the upper respiratory tract that cause multiple mucosal infections, including sinusitis, conjunctivitis, persistent bacterial bronchitis as well as acute and chronic otitis media (OM).[1] In the United States, OM is a major cause of visits to primary care physicians, with socioeconomic direct costs measured in billions of dollars per year.[2] NTHi is frequently linked to recurrent OM infections, and infections recurring less than two weeks after the completion of antibiotic therapy have largely been attributed to the same bacterial strain.[3–4] This suggests that a subpopulation of NTHi can survive antibiotic therapy and reseed the middle ear.

Toxin-Antitoxin (TA) systems are widely encoded by bacteria to enable a rapid response to environmental stressors, including antibiotics and the host immune system, and are implicated in facilitating a state of induced dormancy.[5] These systems are comprised of a toxin that can arrest bacterial growth and an antitoxin that inhibits the toxin during normal growth conditions. Upon induction, toxins rapidly arrest growth by affecting membrane integrity and inhibiting cellular processes, including cell division, DNA replication and protein translation.[6–10] The relevance of TA systems to pathogenicity is supported by a positive correlation between the virulence capacity of a bacterial species and the number of TA systems in its genome.[11] As an example, virulent *Mycobacterium tuberculosis* strains encode at least seventy-nine TA modules; however, the non-pathogenic species *Mycobacterium smegmatis* encodes only four.[12] Six types of TA systems have been described and are classified according to the nature of the antitoxin and the mechanism by which it inhibits the activity of the toxin.[13] For type II TA systems, both the antitoxin and toxin components are proteins, the latter of which is often a ribonuclease enzyme.[14–15] The largest subfamily of type II TA systems is VapBC (virulence associated proteins B and C) of which the toxins contain a highly-conserved PIN (PilT N-terminus) domain with magnesium- or manganese-dependent ribonuclease activity.[16] Within a small genome of approximately 2 Mbp, NTHi maintains two *vapBC* modules designated as *vapBC-1* and *vapBC-2*. The *vapBC-1* locus was shown to be critical for NTHi survival during infections both *in vivo* and *ex vivo*[17] and the VapC1 toxin functions as a potent ribonuclease that degrades both NTHi and *Escherichia coli* total RNA, including ribosomal RNA,[18] tRNA[19],

and has significant activity against the commercial RnaseAlert substrate (Integrated DNA Technologies). Low sequence homology was observed between *vapBC-1* and *vapBC-2.* VapC-2 lacks two of the four conserved aspartic acid residues implicated in ribonuclease activity and is not predicted to contribute significantly to NTHi persistence *in vitro* or *in vivo*. In a primary human respiratory tissue model at the air-liquid interface, survival of the 86–028NP Δ*vapBC-1* strain was significantly reduced compared to the wild-type strain.[17, 20] An NTHi Δ*vapBC-1* strain complemented in *cis* with a TA module at an ectopic site on the chromosome enabled functional characterizations of toxin point mutations in tandem with the wild-type antitoxin under control of the native *vapBC-1* promoter and in single copy. Point mutations to conserved PIN domain residues resulted in significantly reduced NTHi survival compared to the wild-type toxin in a primary human respiratory tissue model.[20] This data directly links the ribonuclease activity of VapC1 to the survival of NTHi in *ex vivo* models of infection. In the chinchilla model of acute OM, NTHi Δ*vapBC-1* mutants survived at 3% of wild-type parent strain levels.[17] Therefore, in the context of OM, the pharmacological inhibition of VapC1 ribonuclease activity might prevent the induction of NTHi growth arrest, persistence and survival during antibiotic therapy. More broadly, the PIN domain is highly conserved,[16, 21] suggesting that inhibitors of VapC1 might show activity against the VapC toxins of other bacteria.

To our knowledge, no inhibitors of VapC1 have been reported; however, a crystal structure of the VapBC-1 complex from NTHi was determined recently.[20] This structure provides atomic-resolution details of the intermolecular interactions enabling inhibition of VapC1 by VapB1. Furthermore, the structure enables structure-based approaches to discover small molecule inhibitors, including virtual screening. However, the lack of a known VapC1 small molecule inhibitor posed a substantial challenge to typical rational design approaches. In this study, we successfully leveraged scaffold hopping[22] by building pharmacophore models from structural features of a VapB1 fragment to identify potential inhibitors of VapC1 through virtual screening. Many of the small molecules identified by this virtual screen were confirmed to inhibit VapC1 ribonuclease activity *in vitro*.

Materials and Methods

VapBC-1 structure preparation:

The crystal structure coordinates of VapBC-1 from nontypeable *Haemophilus influenzae* were downloaded from the Protein Data Bank (www.rcsb.org, PDB ID: 6NKL). Structure preparation was carried out using MOE (version 2019.0102) from the Chemical Computing Group (CCG) to correct structural issues and protonate the structure with optimized positions. The protonated structure was energy minimized using the force field of Amber12EHT (https://www.chemcomp.com/).

Pharmacophore generation and ROCS shape-based mapping:

The structure of VapB1 was truncated such that only the residues in helix α2 interacting with VapC1 were maintained. The pharmacophore query was generated using vROCS (version 3.4.0) from OpenEye Inc. and the primary chemical features contributing to the VapC1:helix α2 interaction were selected. The NCATS small molecule conformational

library was enumerated using OMEGA2 from OpenEye Inc., with an energy window (eWindow) of 5 kcal, root mean square (RMS) Cartesian distance of 0.6 Å, and maximum conformers of 50. ROCS screening was carried out on a Linux cluster with 37 CPUs.

Molecular docking:

The small molecule hits from ROCS screening were subjected to molecular docking. The binding mode of each input molecule was predicted using the Triangle Matcher method in MOE and the thirty best poses were selected according to London dG scores, which estimated the free energy of each pose. The thirty poses were further refined with the Induced Fit method, allowing limited flexibility for the sidechains of VapC1 at the ligand binding site. Finally, the three refined poses with the best Generalized-Born Volume Integral/Weighted Surface Area (GBVI/WSA) dG scores, where solvation energy was taken into consideration, were output and rank-ordered for cherry-picking.

SplitLuc cellular thermal shift assay:

E. coli HST08 Stellar cells (Takara Bio) containing an arabinose-inducible VapC1 plasmid encoding a carboxy-terminal SplitLuc tag (86b, Gly-Ser-HiBiT-Gly-Ser) were selected using chloramphenicol at 20 mg/mL (Teknova, cat#C0312). A culture was inoculated 24 h prior to the assay from glycerol stocks and incubated at 37 °C with shaking (at 250 rpm) overnight. After 16 h, the cultures were diluted to 0.1 OD_{600} and grown to 0.2 – 0.3 OD_{600} with shaking at 37 °C. An equal volume of LB broth containing 20 mg/mL chloramphenicol was added with either a vehicle control (DMSO) or arabinose for a final concentration of 0.05% to induce VapC1 expression. VapC1 inhibitor stock solutions were added for a final concentration of 30 μM, and the samples were incubated at 37 °C with shaking for 3 h. Cell culture aliquots of 30 μL were transferred to PCR tubes and heated for 3.5 min to 37 – 75 °C using an Applied Biosystems Veriti 96 well thermal cycler (ThermoFisher Scientific cat#447907). Cells were lysed by adding 30 μL of B-PER II (ThermoFisher Scientific cat#78260)and the samples were incubated at room temperature for 15 min. Cell lysates were transferred to a white, low volume 384-well plate (Corning cat#3826) and an equal volume of luciferase substrate was added for final concentrations of 0.5X furimazine (Promega NanoGlo substrate, cat#N113A and 100 nM recombinant 11S (Genscript). Luminescence was measured using a ViewLux uHTS microplate imager (PerkinElmer) equipped with clear filters.

Bacterial growth assay:

E. coli HST08 Stellar cells (Takara Bio) containing VapC1 or VapC1 and VapB1 expression vectors were cultured in LB broth containing 20 mg/mL chloramphenicol (Teknova C0312) or 20 mg/mL chloramphenicol with 100 mg/mL carbenicillin (Teknova C8001), respectively. Cultures were inoculated 24 h prior to the assay from glycerol stocks and incubated at 37 °C with shaking at 250 rpm overnight. After 16 h, the cultures were diluted to 0.1 OD_{600} and then grown to 0.2 – 0.3 OD_{600} with shaking at 37 °C. An equal volume of LB broth containing antibiotic was added with either vehicle (DMSO) or arabinose to a final concentration of 0.05%. For co-expression of the antitoxin VapB1, isopropyl β-D-thiogalactoside (IPTG, Sigma cat#I6758) was added to a final concentration of 0.5 mM. VapC1 inhibitor stock solutions were added for a final concentration of 30 μM, and the

samples were incubated at 37 °C with shaking at 250 rpm for 3 h. The OD_{600} was measured using a spectrophotometer (DeNovix, DS-11 model).

Biochemical VapC1 ribonuclease activity assay:

The VapC1 ribonuclease activity assay was performed in black, medium binding, solid bottom 1,536-well plates (Greiner, Catalog 789176-F). First, 13 nL of test compounds, positive control aurintricarboxylic acid (Sigma, Catalog A1895–25G) or vehicle control DMSO were either transferred by pin tool (Kalypsis) or acoustic dispensing (Labcyte Inc., Echo 655) into 3 μL of 1X RNaseAlert reaction buffer (Integrated DNA Technologies, Lot 238712) prepared from a 10X stock solution using Nuclease Free Water (Integrated DNA Technologies, Catalog 11–05-01–04) with 494 nM purified VapC1 [296 nM, final concentration]. The assay plates were incubated for 30 min at room temperature with the controls and test compounds. The VapC1 reaction was initiated by the addition of 2 μL containing 250 nM [100 nM, final concentration] RNaseAlert (a custom version of the commercial product with a 5' Cy5 fluorophore and a 3' Iowa Black RQ quencher, Integrated DNA Technologies) in 1X RNaseAlert reaction buffer. Fluorescence measurements were made (λEx 618 nm, λEm 671 nm) with a ViewLux uHTS microplate imager (PerkinElmer). The exposure time was 4 s with an excitation energy of 45,396.0, readout speed of 2 μs, readout gain of 6.6X, 2X image binning, flat field correction, bias correction, bias structure correction, and cosmic ray detection. The narrow band interference filter for excitation was 618 nm ± 4 nm (618/8) and the emission filter was 671 nm ± 4 nm (671/8). Fluorescence was measured immediately following the addition of substrate and at 75 min. VapC1 activity was measured as the change between initial and final relative fluorescence values.

Results and Discussion

Analysis of a VapBC-1 complex structure:

A recently reported crystal structure of a NTHi VapBC-1 hetero-tetramer complex revealed the interfaces between both the VapC1-VapC1 homodimer and the VapC1-VapB1 heterodimer (Figure 1a).[20] The homodimer interface is flat and lipophilic with an area greater than 1,000 $Å^2$ (Figure 1b). In contrast, the interface between VapC1 and VapB1 appears to be more amenable to disruption by small molecules, as two α-helices from VapB1 lie in a long cleft on the surface of VapC1 (Figure 1b and 1c). Both VapB1 α–helices are amphipathic (Figure 2), which is a feature commonly observed in protein-protein interactions, for example the interactions between MDM2-p53[23] and BCLxl-BAK.[24] The lipophilic faces are buried in a cleft on the surface of VapC1, forming a vast interface area of 1,662 $Å^2$.[20] Both pockets on the surface of VapC1 that accommodate each of the two VapB1 α–helices are potential allosteric binding sites for small molecules to interfere with the VapC1 ribonuclease activity. However, we selected helix α2 (F^{56}DETFIQALE^{65}) near the C-terminal tail as the target, because this region is proximal to the VapC1 catalytic site (the red patch in Figure 1d). The catalytic core of VapC1, also known as the "catalytic triad", is composed of three strictly conserved acidic residues, D6, E43, and D99. The VapBC-1 complex crystal structure clearly reveals that binding of VapB1 blocks substrate access to the "catalytic triad" site (Figure 1a), thereby inhibiting the ribonuclease activity of VapC1.

Therefore, a small molecule occupying the helix α2 binding site is hypothesized to mimic the antitoxin function of VapB1 to inhibit VapC1.

A pharmacophore model generated from the VapB1 peptide structure:

Pharmacophore-based virtual screening provides a highly efficient tool,[25] which is capable of screening a trillion compounds in a time frame of hours using FastROCS.[26] Pharmacophore-based virtual screening also enables scaffold hopping from peptide or protein structures to small molecules.[22, 27] The goal of this research was to discover small molecules based on the VapB1 helix α2 peptide structure that bind VapC1 and mimic the hydrophobic interactions of helix α2 with VapC1. Because helix α2 is a large polypeptide of 10 amino acids, with a molecular weight exceeding 1,300 Daltons, a pharmacophore model based on the entire VapB1 helix α2 structure is inappropriate for the discovery of small molecules. Instead, a truncated structure of helix α2, which captures the key intermolecular interactions, was adopted for pharmacophore construction. The VapBC-1 complex crystal structure shows that the hydrophobic face of the helix α2 peptide primarily contributes to the intermolecular interactions. Therefore, the four VapB1 hydrophobic residues whose side chains are buried in the hydrophobic cleft on the VapC1 surface (F56, F60, I61, and L64, Figure 3a) were selected as key functional groups for query construction. The pharmacophore query was comprised of the shape feature defined by the hydrophobic face of VapB1 helix α2, together with four chemical features—two hydrophobes for I61 and L64 and two hydrophobes with rings for F56 and F60, as shown in Figure 3b.

Novel inhibitors identified by ROCS shape-based mapping and structure-based virtual screening:

The National Center for Advancing Translational Sciences (NCATS) collection of nearly a halfmillion small molecules was pre-prepared using Pipeline Pilot (https://www.3ds.com/products-services/biovia/products/data-science/pipeline-pilot/) to remove salts and redundant molecules as well as to standardize stereochemistry and formal charges. The conformational library was enumerated for the resulting 404,592 small molecules using OMEGA2 from OpenEye Inc. (https://docs.eyesopen.com/applications/omega/index.html), with energy window (eWindow) set to 5 kcal, root mean square (RMS) Cartesian distance set to 0.6 Å, and maximum conformers set to 50. The Rapid Overlay of Chemical Structures (ROCS) is a virtual screening tool to score and rank-order a compound library based on the alignment of shape similarities and chemical features defined in a query.[28] Screening with ROCS was carried out on a Linux cluster and finished in 977 seconds with 37 CPUs. The best 1,500 hit molecules were then docked into the VapC1:helix α2 interface using an induced fit algorithm installed in MOE (http://www.chemcomp.com/). Dock solutions of the top 200 compounds with the best predicted binding energies were then prepared and tested in a biochemical assay.

Confirmation of virtual screening hits with a biochemical VapC1 ribonuclease activity assay:

A biochemical VapC1 ribonuclease activity assay was used to evaluate hits from the virtual screen. This sensitive assay leverages a custom RNaseAlert substrate containing a 5’ Cy5 fluorophore and a 3’ Iowa Black® RQ quencher (Integrated DNA Technologies, Coralville,

IA). Enzymatic cleavage of the custom RNA substrate by VapC1 separates the fluorophore from the quencher, resulting in a real-time kinetic red-fluorescence readout of ribonuclease activity. The assay is robust with a Z'-factor value of 0.92. Eight of 200 selected compounds from the virtual screen inhibited VapC1 ribonuclease activity with IC_{50} values ranging between 1.3 μM and 20 μM, which is a 4% confirmation rate (Figure 4, Table S1). The active compounds can be classified into two chemotypes, the majority of which are phenylpyridiones. These phenylpyridiones were developed internally as part of a project to target isocitrate dehydrogenase type 1 (IDH1).[29–30] Therefore the biochemical testing was extended to include all phenylpyridiones from the IDH1 project, and identified twenty additional VapC1 inhibitors.

Characterization of confirmed VapC1 ribonuclease inhibitors in cell-based assays:

Given the structure activity relationships among members of the phenylpyridone chemotype in the biochemical VapC1 ribonuclease activity assay data (Figure 4a), seven were advanced for evaluation in cell-based assays (Figure 4c). The compounds were selected based on their potency and structural diversity within the chemotype. The capacity of these seven biochemical inhibitors to engage VapC1 within bacterial cells was assessed using a SplitLuc cellular thermal shift assay (CETSA). All compounds decreased the thermal stability of the enzyme to some extent, suggesting intracellular target engagement (Figure 4c). To examine whether the VapC1 biochemical inhibitors also demonstrate activity within bacteria, an *E. coli* growth assay was used. As expected, the induced expression of VapC1 in *E. coli* inhibited bacterial growth, whereas co-expression of the antitoxin VapB1 rescued growth. In this cell-based activity assay, none of the compounds rescued the growth inhibition associated with VapC1 expression (Figure 4d). These results suggested that the compounds did not inhibit VapC1 enzymatic activity to a level that is sufficient to reverse the growth phenotype.

In silico evaluation of VapC1 ribonuclease inhibitors:

The docking models of hit compounds indicated that shape complementarity and hydrophobic interactions are the major contributors to ligand binding affinities, while contributions from electrostatic interactions are very limited (Figure 5). An analysis of intermolecular interaction energies confirmed this observation—*Van der Waals* energy accounts for over 90% of the non-covalent binding energy. Intermolecular recognition dominated by *Van der Waals* force is the hallmark of protein-protein interactions (PPI) where amphipathic helical structures are involved in the PPI interfaces, as exemplified by p53-MDM2 and the MDM2 inhibitor Nutlin-3.[31–32] In the current study, the backbone amides form hydrogen bonds with each other, while the hydrophobic side chains of VapB1 helix α2 make the major contributions to the PPI (Figure 3). The biochemically confirmed small molecule inhibitors of VapC1 are predicted to imitate the VapB1 helix α2 interactions by burying hydrophobic moieties into hydrophobic pockets on the surface of VapC1 and allowing hydrophilic moieties to be solvent exposed (Figure 5b and 5d). In summary, by converting key peptide functional groups involved in the PPI to a pharmacophore query, multiple small molecule inhibitors were successfully identified which might mimic the native peptide-protein interactions (Figure 6).

Conclusion

In this report, scaffold hopping from a peptide structure to a pharmacophore query enabled a virtual screen that identified inhibitors of the ribonuclease VapC1 from NTHi without any prior structural knowledge of small molecule inhibitors. Nontypeable *Haemophilus influenzae* are clinically important bacteria that cause a range of mucosal infections and exacerbations of chronic obstructive pulmonary disease. Drug resistant NTHi strains are increasingly isolated from difficult-to-treat respiratory infections and a heightened surveillance of NTHi as an emerging pathogen has been proposed.[1] Bacterial TA systems have been implicated in persistence and non-specific tolerance to antibiotics, enabling bacterial survival of human infections and antibiotic therapy.[5, 33] In this context, TA systems have been identified as a potential therapeutic target.[34–37] NTHi is an ideal organism for testing this therapeutic hypothesis because the VapBC-1 module has been shown to significantly increase survival during infections *in vivo*[17]. To our knowledge, no small molecule inhibitors of VapC1 have been described; however, structural studies were reported of VapC1 bound to its native inhibitor, antitoxin VapB1.[20] Scaffold hopping from a VapB1 peptide structure to small molecules was successfully achieved through extracting key chemical features from the VapB1 helix α2 peptide together with shape complementarity requirements to generate a pharmacophore query. Virtual screening was performed with the NCATS compound library of over 400,000 compounds using ROCS and molecular docking. This approach enabled the discovery of small molecule VapC1 ribonuclease inhibitors for the first time, with 8 of the top 200 hits demonstrating activity in a biochemical assay. Following a structural analysis of the experimentally confirmed hits, 20 additional inhibitors were identified from the phenylpyridione chemotype. Seven validated inhibitors were selected for further evaluation in cell-based assays due to their structure activity relationships and biochemical potencies. All seven compounds destabilized VapC1 in a Splitluc CETSA performed with *E. coli*. These data indicated that the compounds both enter bacteria and engage their intracellular target. The *E. coli* growth inhibition assay did not detect any ability of the seven compounds to rescue the growth inhibition resulting from VapC1 expression. However, this result might be anticipated for compounds that have not been optimized by medicinal chemistry for intracellular VapC1 inhibition. Despite entering bacteria, the compounds likely did not achieve a sufficient intracellular concentration or inhibition of VapC1 to rescue the growth arrest to the level of the VapB1 control. Therefore, these VapC1 inhibitors might serve as a starting point for the preclinical development of an adjuvant therapeutic for use against NTHi. More broadly, these inhibitors might be further developed to target the VapC toxins of other pathogenic bacteria.

Supplementary Material

Refer to Web version on PubMed Central for supplementary material.

Acknowledgment:

This work was supported by the Intramural Research Programs of the National Center for Advancing Translational Sciences, National Institutes of Health.

Data and Software Availability:

The PDB files were downloaded from the RCSB protein data bank (https://www.rcsb.org). All the output data and structures of the hit compounds have been provided in the article and Supporting Information. The software package of PyMOL (https://pymol.org) was used to prepare Figure 1, 3 and 5. Preparation of the compound library for virtual screening was carried out by using Pipeline Pilot (https://www.3ds.com/products-services/biovia/products/data-science/pipeline-pilot/). Virtual screening was performed using ROCS3.4.0, vROCS3.4.0, and OMEGA2 by OpenEye Inc. (https://www.eyesopen.com). Molecular docking was performed using MOE (https://www.chemcomp.com). All the software were purchased and licensed to the NCATS.

References:

1. Van Eldere J; Slack MP; Ladhani S; Cripps AW, Non-typeable Haemophilus influenzae, an under-recognised pathogen. Lancet Infect Dis 2014, 14 (12), 1281–1292. [PubMed: 25012226]
2. Grevers G; First International Roundtable, E. N. T. M. G., Challenges in reducing the burden of otitis media disease: an ENT perspective on improving management and prospects for prevention. Int J Pediatr Otorhinolaryngol 2010, 74 (6), 572–577. [PubMed: 20409595]
3. Barenkamp SJ; Shurin PA; Marchant CD; Karasic RB; Pelton SI; Howie VM; Granoff DM, Do children with recurrent Haemophilus influenzae otitis media become infected with a new organism or reacquire the original strain? J Pediatr 1984, 105 (4), 533–537. [PubMed: 6332891]
4. Leibovitz E; Greenberg D; Piglansky L; Raiz S; Porat N; Press J; Leiberman A; Dagan R, Recurrent acute otitis media occurring within one month from completion of antibiotic therapy: relationship to the original pathogen. Pediatr Infect Dis J 2003, 22 (3), 209–216. [PubMed: 12634580]
5. Coussens NP; Daines DA, Wake me when it's over - Bacterial toxin-antitoxin proteins and induced dormancy. Exp Biol Med (Maywood) 2016, 241 (12), 1332–1342. [PubMed: 27216598]
6. Zhang Y; Zhang J; Hoeflich KP; Ikura M; Qing G; Inouye M, MazF cleaves cellular mRNAs specifically at ACA to block protein synthesis in Escherichia coli. Mol Cell 2003, 12 (4), 913–923. [PubMed: 14580342]
7. Christensen SK; Gerdes K, RelE toxins from bacteria and Archaea cleave mRNAs on translating ribosomes, which are rescued by tmRNA. Mol Microbiol 2003, 48 (5), 1389–1400. [PubMed: 12787364]
8. Tan Q; Awano N; Inouye M, YeeV is an Escherichia coli toxin that inhibits cell division by targeting the cytoskeleton proteins, FtsZ and MreB. Mol Microbiol 2011, 79 (1), 109–118. [PubMed: 21166897]
9. Aakre CD; Phung TN; Huang D; Laub MT, A bacterial toxin inhibits DNA replication elongation through a direct interaction with the beta sliding clamp. Mol Cell 2013, 52 (5), 617–628. [PubMed: 24239291]
10. Pecota DC; Osapay G; Selsted ME; Wood TK, Antimicrobial properties of the Escherichia coli R1 plasmid host killing peptide. J Biotechnol 2003, 100 (1), 1–12. [PubMed: 12413781]
11. Georgiades K; Raoult D, Genomes of the most dangerous epidemic bacteria have a virulence repertoire characterized by fewer genes but more toxin-antitoxin modules. PLoS One 2011, 6 (3), e17962.
12. Sala A; Bordes P; Genevaux P, Multiple toxin-antitoxin systems in Mycobacterium tuberculosis. Toxins (Basel) 2014, 6 (3), 1002–1020. [PubMed: 24662523]
13. Harms A; Brodersen DE; Mitarai N; Gerdes K, Toxins, Targets, and Triggers: An Overview of Toxin-Antitoxin Biology. Mol Cell 2018, 70 (5), 768–784. [PubMed: 29398446]
14. Masuda H; Inouye M, Toxins of Prokaryotic Toxin-Antitoxin Systems with Sequence-Specific Endoribonuclease Activity. Toxins (Basel) 2017, 9 (4).
15. Page R; Peti W, Toxin-antitoxin systems in bacterial growth arrest and persistence. Nat Chem Biol 2016, 12 (4), 208–214. [PubMed: 26991085]

16. Arcus VL; McKenzie JL; Robson J; Cook GM, The PIN-domain ribonucleases and the prokaryotic VapBC toxin-antitoxin array. Protein Eng Des Sel 2011, 24 (1–2), 33–40. [PubMed: 21036780]
17. Ren D; Walker AN; Daines DA, Toxin-antitoxin loci vapBC-1 and vapXD contribute to survival and virulence in nontypeable Haemophilus influenzae. BMC Microbiol 2012, 12, 263. [PubMed: 23157645]
18. Daines DA; Wu MH; Yuan SY, VapC-1 of nontypeable Haemophilus influenzae is a ribonuclease. J Bacteriol 2007, 189 (14), 5041–5048. [PubMed: 17496075]
19. Walling LR; Butler JS, Homologous VapC Toxins Inhibit Translation and Cell Growth by Sequence-Specific Cleavage of tRNA(fMet). J Bacteriol 2018, 200 (3).
20. Molinaro AL; Kashipathy MM; Lovell S; Battaile KP; Coussens NP; Shen M; Daines DA, Crystal Structure of VapBC-1 from Nontypeable Haemophilus influenzae and the Effect of PIN Domain Mutations on Survival during Infection. J Bacteriol 2019, 201 (12).
21. Bendtsen KL; Brodersen DE, Higher-Order Structure in Bacterial VapBC Toxin-Antitoxin Complexes. Subcell Biochem 2017, 83, 381–412. [PubMed: 28271484]
22. Sun H; Tawa G; Wallqvist A, Classification of scaffold-hopping approaches. Drug Discov Today 2012, 17 (7–8), 310–324. [PubMed: 22056715]
23. Kussie PH; Gorina S; Marechal V; Elenbaas B; Moreau J; Levine AJ; Pavletich NP, Structure of the MDM2 oncoprotein bound to the p53 tumor suppressor transactivation domain. Science 1996, 274 (5289), 948–953. [PubMed: 8875929]
24. Wysoczanski P; Mart RJ; Loveridge EJ; Williams C; Whittaker SB; Crump MP; Allemann RK, NMR solution structure of a photoswitchable apoptosis activating Bak peptide bound to Bcl-xL. J Am Chem Soc 2012, 134 (18), 7644–7647. [PubMed: 22515821]
25. Sun H, Pharmacophore-based virtual screening. Curr Med Chem 2008, 15 (10), 1018–1024. [PubMed: 18393859]
26. Grebner C; Malmerberg E; Shewmaker A; Batista J; Nicholls A; Sadowski J, Virtual Screening in the Cloud: How Big Is Big Enough? J Chem Inf Model 2020, 60 (9), 4274–4282. [PubMed: 31682421]
27. Sun H; Greeley DN; Chu XJ; Cheung A; Danho W; Swistok J; Wang Y; Zhao C; Chen L; Fry DC, A predictive pharmacophore model of human melanocortin-4 receptor as derived from the solution structures of cyclic peptides. Bioorg Med Chem 2004, 12 (10), 2671–2677. [PubMed: 15110848]
28. Rush TS 3rd; Grant JA; Mosyak L; Nicholls A, A shape-based 3-D scaffold hopping method and its application to a bacterial protein-protein interaction. J Med Chem 2005, 48 (5), 1489–1495. [PubMed: 15743191]
29. Urban DJ; Martinez NJ; Davis MI; Brimacombe KR; Cheff DM; Lee TD; Henderson MJ; Titus SA; Pragani R; Rohde JM; Liu L; Fang Y; Karavadhi S; Shah P; Lee OW; Wang A; McIver A; Zheng H; Wang X; Xu X; Jadhav A; Simeonov A; Shen M; Boxer MB; Hall MD, Assessing inhibitors of mutant isocitrate dehydrogenase using a suite of pre-clinical discovery assays. Sci Rep 2017, 7 (1), 12758. [PubMed: 28986582]
30. Rohde JM; Karavadhi S; Pragani R; Liu L; Fang Y; Zhang W; McIver A; Zheng H; Liu Q; Davis MI; Urban DJ; Lee TD; Cheff DM; Hollingshead M; Henderson MJ; Martinez NJ; Brimacombe KR; Yasgar A; Zhao W; Klumpp-Thomas C; Michael S; Covey J; Moore WJ; Stott GM; Li Z; Simeonov A; Jadhav A; Frye S; Hall MD; Shen M; Wang X; Patnaik S; Boxer MB, Discovery and Optimization of 2H-1lambda(2)-Pyridin-2-one Inhibitors of Mutant Isocitrate Dehydrogenase 1 for the Treatment of Cancer. J Med Chem 2021, 64 (8), 4913–4946. [PubMed: 33822623]
31. Fry DC; Wartchow C; Graves B; Janson C; Lukacs C; Kammlott U; Belunis C; Palme S; Klein C; Vu B, Deconstruction of a nutlin: dissecting the binding determinants of a potent protein-protein interaction inhibitor. ACS Med Chem Lett 2013, 4 (7), 660–665. [PubMed: 24900726]
32. Vu B; Wovkulich P; Pizzolato G; Lovey A; Ding Q; Jiang N; Liu JJ; Zhao C; Glenn K; Wen Y; Tovar C; Packman K; Vassilev L; Graves B, Discovery of RG7112: A Small-Molecule MDM2 Inhibitor in Clinical Development. ACS Med Chem Lett 2013, 4 (5), 466–469. [PubMed: 24900694]
33. Wood TK, Combatting bacterial persister cells. Biotechnol Bioeng 2016, 113 (3), 476–483. [PubMed: 26264116]

34. Park SJ; Son WS; Lee BJ, Structural overview of toxin-antitoxin systems in infectious bacteria: a target for developing antimicrobial agents. Biochim Biophys Acta 2013, 1834 (6), 1155–1167. [PubMed: 23459128]

35. Williams JJ; Hergenrother PJ, Exposing plasmids as the Achilles' heel of drug-resistant bacteria. Curr Opin Chem Biol 2008, 12 (4), 389–399. [PubMed: 18625335]

36. Williams JJ; Hergenrother PJ, Artificial activation of toxin-antitoxin systems as an antibacterial strategy. Trends Microbiol 2012, 20 (6), 291–298. [PubMed: 22445361]

37. Chan WT; Balsa D; Espinosa M, One cannot rule them all: Are bacterial toxins-antitoxins druggable? FEMS Microbiol Rev 2015, 39 (4), 522–540. [PubMed: 25796610]

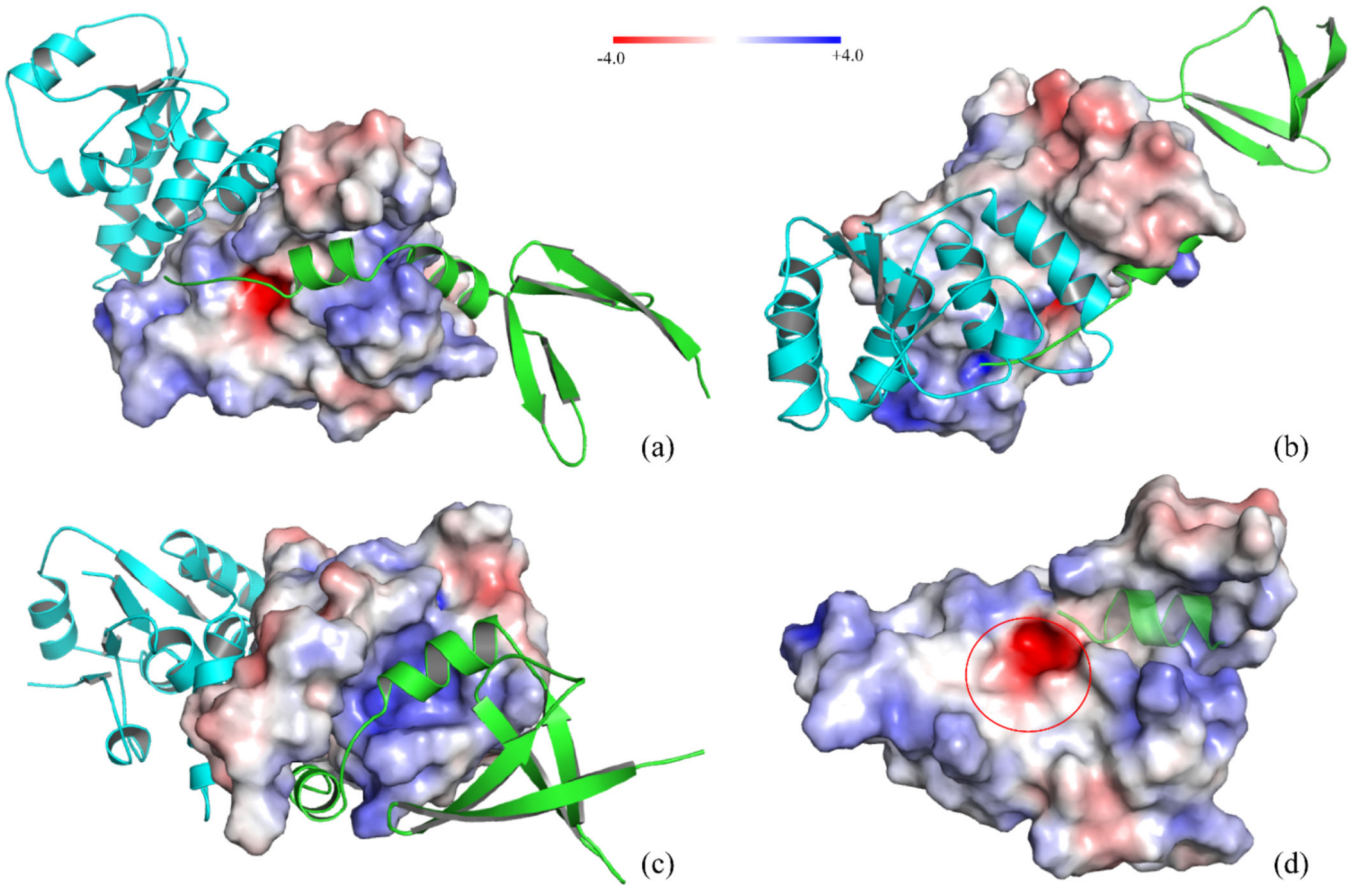

Figure 1.

Structural features of the VapBC-1 complex (PDB ID: 6NKL). (a - c) The VapBC-1 complex is shown from different viewpoints to highlight the homodimeric interactions between VapC1 monomers (shown as a ribbon diagram, *cyan*, and a surface projection colored as a heatmap according to the electrostatic potential, respectively) and heterodimeric interactions with VapB1 helixes α1 and α2 (*green*, ribbon diagram). (d) The helix α2 of VapB1 is adjacent to the catalytic site of VapC1, which is marked by a red circle. All diagrams were generated with the program PyMOL. The scale for the electrostatic potential heatmap is shown at the top of the figure.

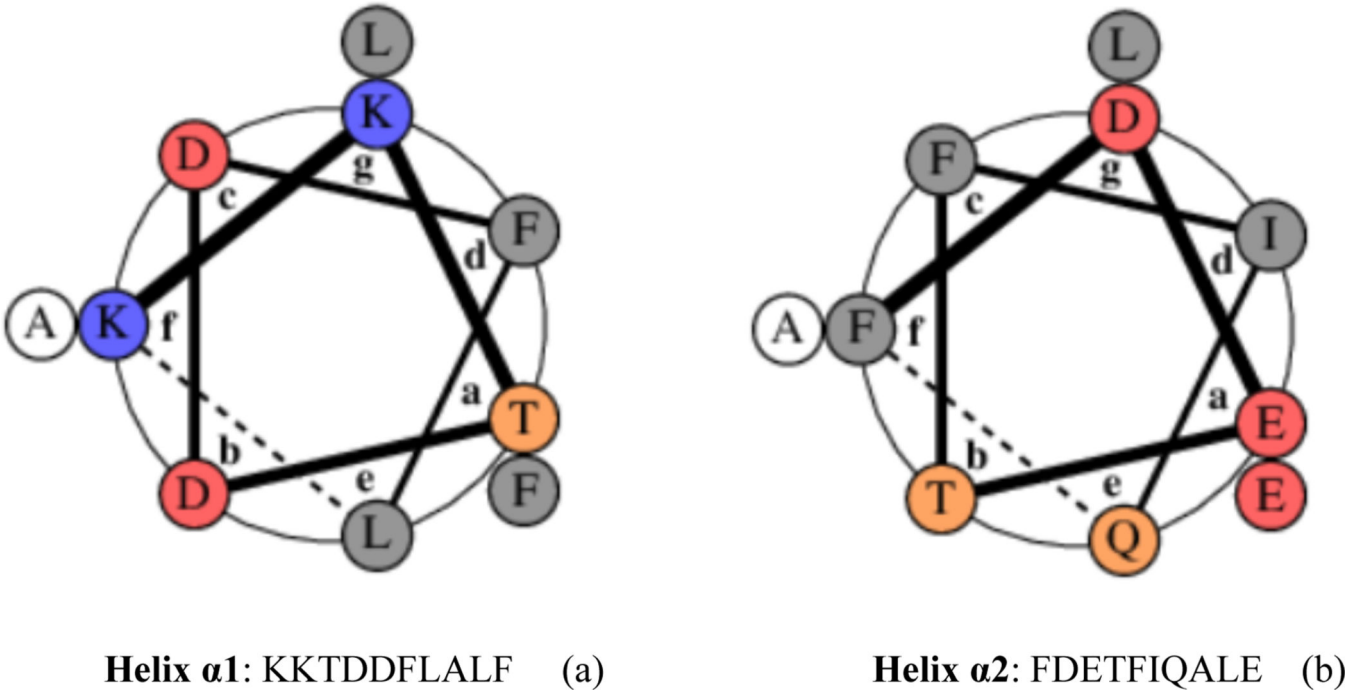

Figure 2.
The amphipathic features of (a) helix α1 and (b) helix α2 shown as wheel diagrams.

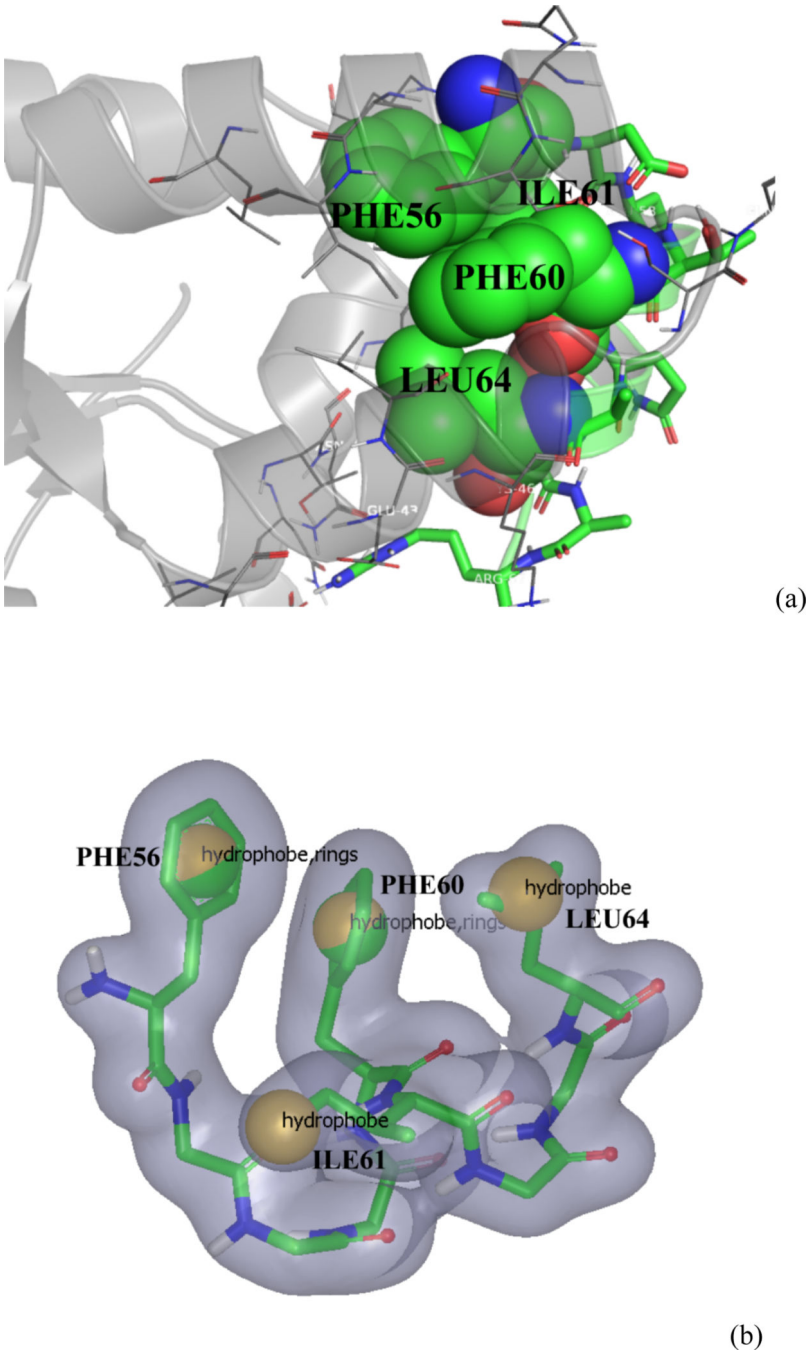

Figure 3.

A space-filling model showing the side chains of the four hydrophobic residues from the amphipathic helix α2 of VapB1. (a) The VapB1 residues F56, F60, I61, and L64 (*green*) primarily contribute to the intermolecular interactions with VapC1 (*gray*, ribbon diagram). (b) The pharmacophore query was defined by the shape of VapB1 helix α2 as well as hydrophobes for I61 and L64 and hydrophobes with rings for F56 and F60.

(a)

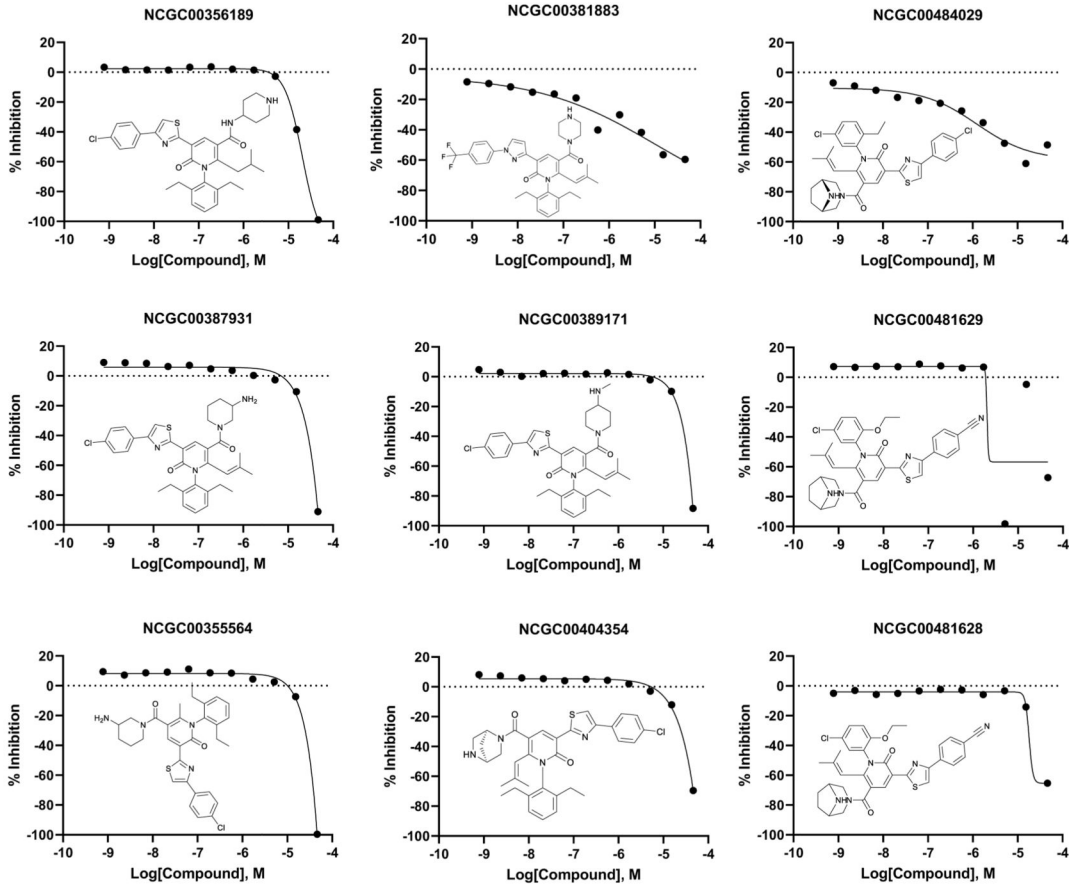

(b)

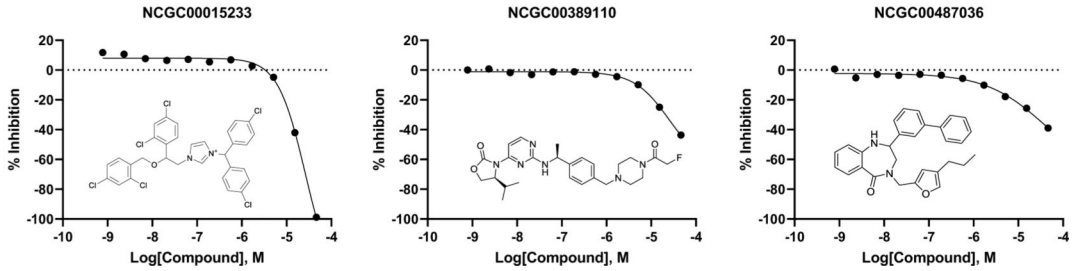

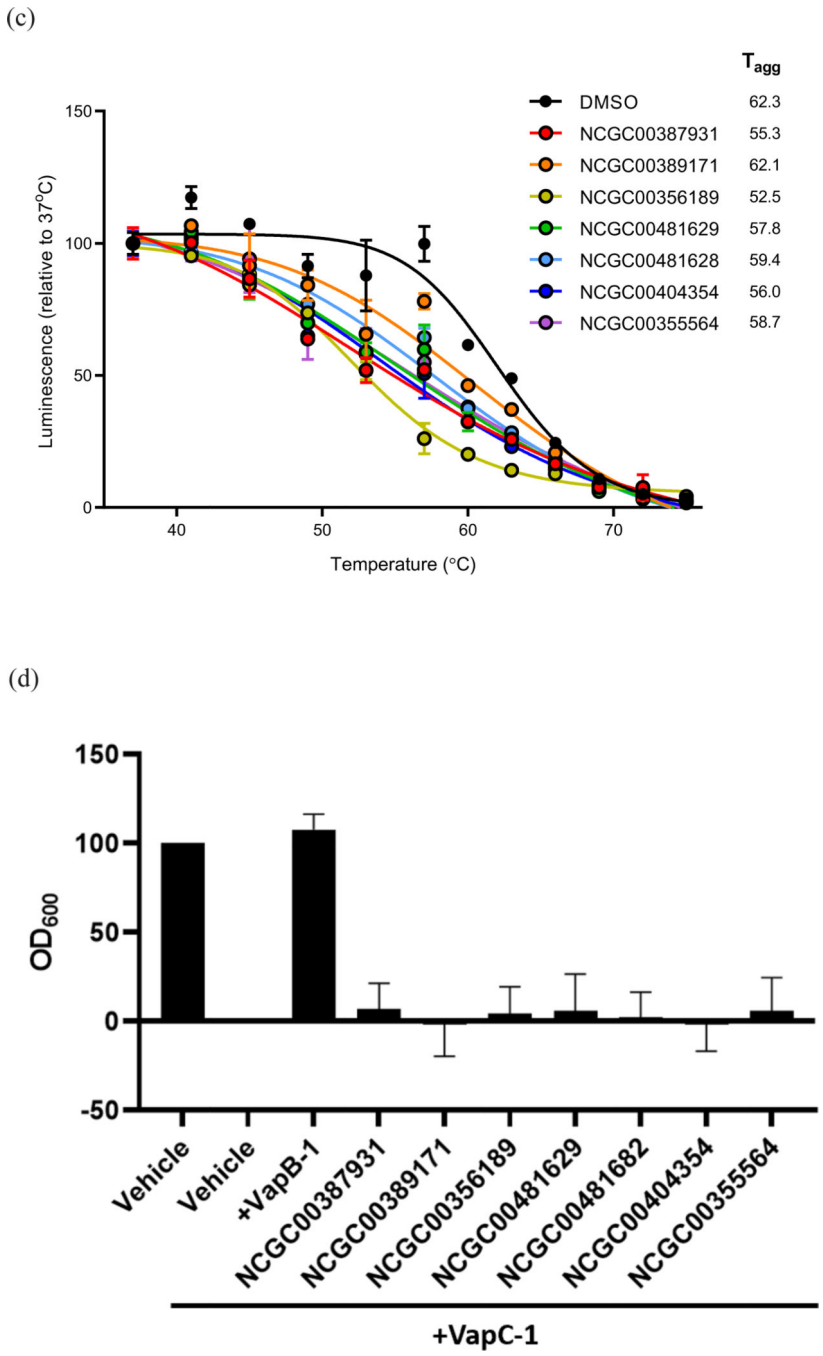

Figure 4.

Evaluation of hit compounds from the virtual screen using biochemical and cell-based assays. (a - b) Dose-dependent inhibition of VapC1 ribonuclease activity is shown for twelve active compounds from (a) The highly enriched 2-pyridone chemotype and (b) Singleton hits. The concentration-response curves span eleven concentrations and maximal VapC1 inhibition ranges between 52% and 100%. (c) The thermal stability of VapC1 was examined in *E. coli* following treatment with seven confirmed VapC1 inhibitors using a SplitLuc Cellular Thermal Shift Assay. Compared to treatment with vehicle (DMSO)

treatment with the VapC1 inhibitors destabilized VapC1 as indicated by their reduced T_{agg} values. (d) Bacterial growth was measured by absorbance (OD_{600}) after 3 hours of VapC1 expression (by an arabinose inducible promoter) ± treatment with vehicle or confirmed VapC1 inhibitors. Growth was normalized to control groups without VapC1 induction (100%) and with VapC1 induction (0%).

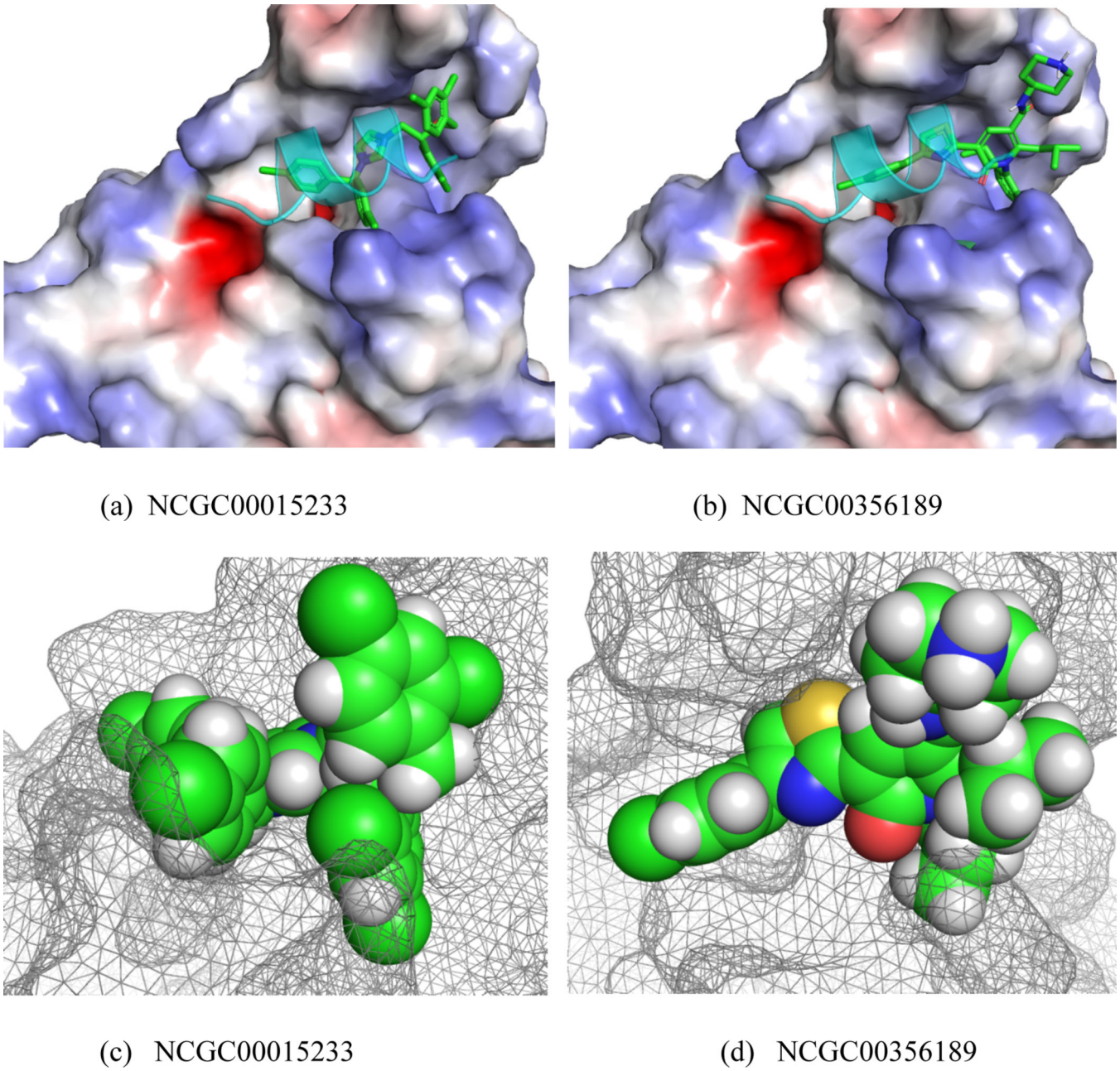

Figure 5.

The predicted conformations of two confirmed VapC1 inhibtors NCGC00015233 (a and c) and NCGC00356189 (b and d) bound to the helix α2 pocket on the surface of VapC1. The ribbon diagrams pictured in (a) and (b) (*cyan*) show the backbone position of the helix α2 polypeptide. The protein surface of VapC1 in (a) and (b) is colored according to eletrostactic potential, while in (c) and (d) it is shown as a mesh surface with space-filling ligands to illustrate the shape complementarity.

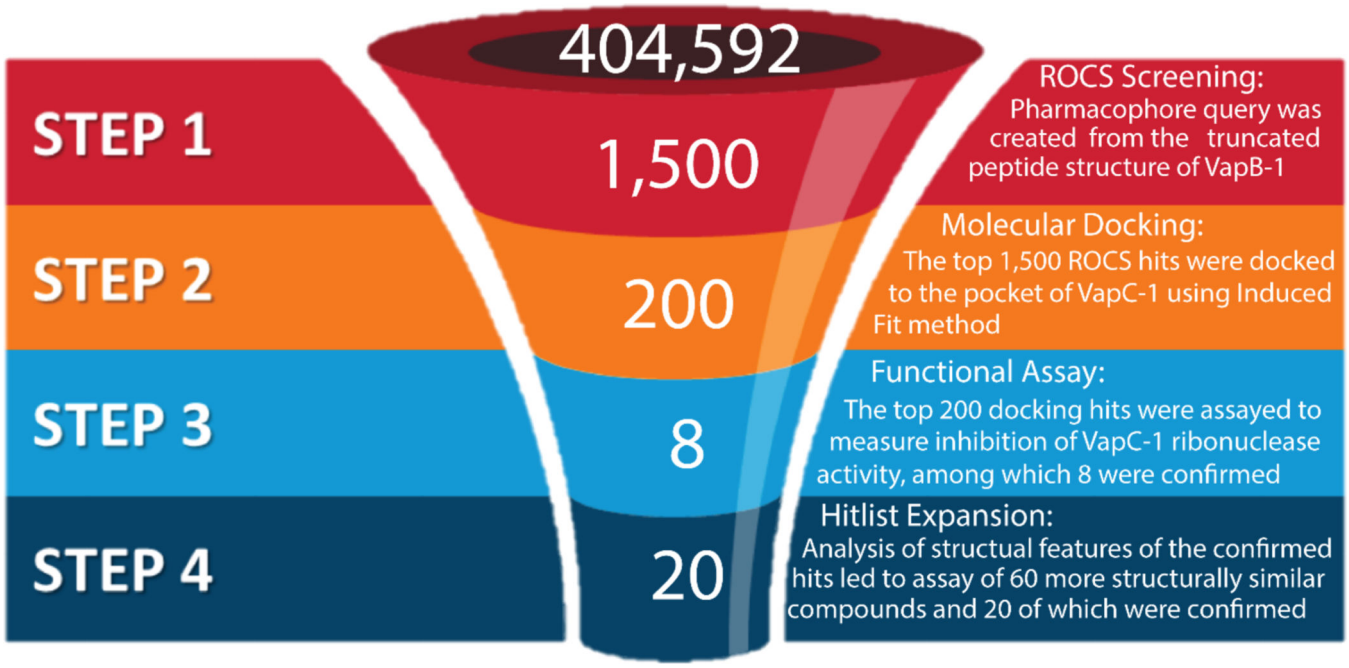

Figure 6.

A workflow to combine two virtual screening methods, shape-based Rapid Overlay of Chemical Structures (ROCS) and energy-based molecular docking, to facilitate scaffold hopping from a peptide structure to small molecule inhibitors. Notably, a post-virtual screening analysis led to an expansion of the hit list.